2022-01-22

Modelling of multi-species transport in concrete under the action of external electric field: Influence of the overpotential at electrode-electrolyte interfaces

Mao, L-X

10.1016/j.jelechem.2022.116079
Journal of Electroanalytical Chemistry
Elsevier BV

Journal of Electroanalytical Chemistry, Available online 22 January 2022, 116079
Received on 3 December 2021, Revised 3 January 2022, Accepted 19 January 2022
https://doi.org/10.1016/j.jelechem.2022.116079

Modelling of multi-species transport in concrete under the action of external electric field: Influence of the overpotential at electrode-electrolyte interfaces

Li-xuan Mao, Long-yuan Li, Boksun Kim

School of Engineering, Computing and Mathematics, University of Plymouth,

Plymouth PL4 8AA, UK

Abstract

The application of external electrical field on concrete structures is widely used to protect it from chloride attack or to evaluate its resistance to chloride penetration in a short period. During these electrochemical processes, the polarization of electrodes placed inside and/or outside of concrete cannot be ignored. This study proposes a numerical model dealing with the mass transport and electrode polarizing process under an externally applied voltage, in which multi-species electromigration, time-varying overpotential and non-equilibrium binding are involved. The Tafel Equation is adopted to express the overpotential at electrode-electrolyte interfaces. The electro-potential boundary changing with overpotential is reset at each time step to obtain the accurate concentration distributions of ionic species. Additionally, benchmarks against third-party experiments are conducted to verify the reliability of the present model. The effects of externally applied voltage, Tafel parameters and initial ionic species concentration on the interaction of overpotential and chloride penetration are also quantitatively examined. The obtained results show that the potential difference between two concrete surfaces is always lower than that applied on electrodes due to the influence of polarization, which has a further impact on the temporal and spatial concentration distributions of ionic species in the pore solution of concrete.

Keywords: Chloride, Electrochemical Process, Polarization, Multi-species Electro-migration, Overpotential.

1. Introduction

The durability and safety of reinforced concrete structures in the salt environment can be significantly influenced by the ingress of chloride ions [1]. The impressed current cathodic protection (ICCP) and electrochemical chloride removal (ECR) techniques are widely used to protect the structures from chloride attack by applying an external electrical field [2-4]. Moreover, the accelerated chloride migration test (ACMT) and rapid chloride migration test (RCM) have been developed to evaluate concrete resistance to chloride penetration in a short period for the durability design and service life prediction of concrete structures [5, 6]. Despite the differences in duration, external electrical field, and objectives, these testing techniques are all built on the same electrochemical principle of accelerating the movement of ionic species in concrete by means of an externally applied electrical field. As shown in Figure 1, under the action of external driving force, chloride ions are transported from the cathode to anode; whereas hydroxyl ions are produced at the cathode and transferred to the anode where they are consumed. Conversely, the cations, such as sodium and potassium ions, move from anode towards to cathode. More importantly, whether or not the electrodes are placed inside the concrete specimen, the overpotential (OP) at electrode-electrolyte interfaces caused by polarization may affect the ionic transport in the pore solution of concrete [7, 8].

In electrochemistry, the overpotential is the potential difference (voltage) between a half-reaction's thermodynamically determined reduction potential and the potential at which the redox event is experimentally observed [9]. The overpotential at the cathode is more negative for the reducing process, and at the anode it is more positive for the oxidizing process. Thus, the externally applied voltage between two electrodes is higher than the actual potential across the concrete specimen.

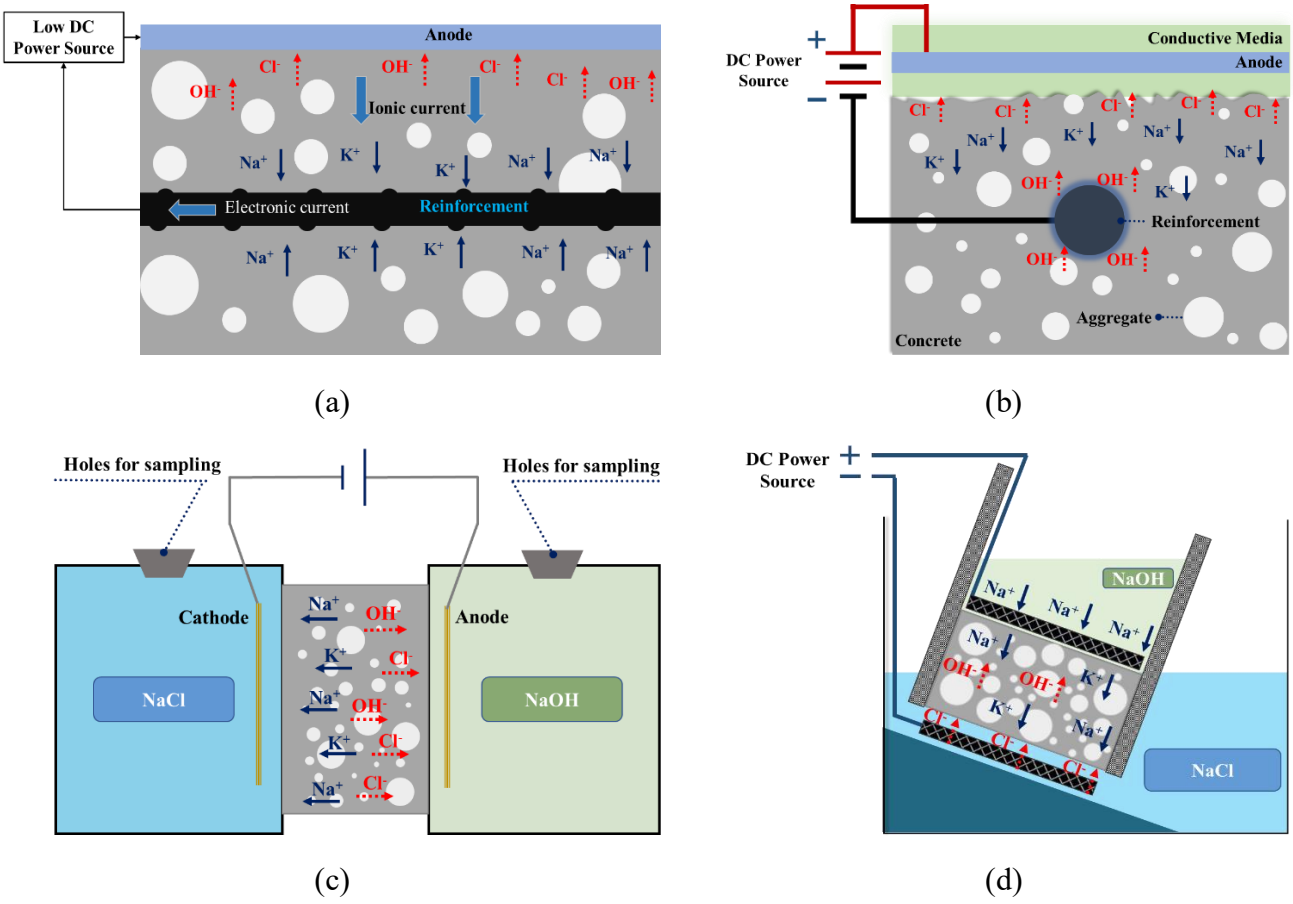

Figure 1 The schematic of different electrochemical processes: (a) Impressed current cathodic protection, (b) Electrochemical chloride removal, (c) Accelerated chloride migration test, (d) Rapid chloride migration test.

For the RCM tests, NT Build 492 reported a fixed overpotential to reflect the impact of polarization on the non-steady-state migration coefficient, which is expressed as:

$$D_{nssm} = \frac{0.0239TL}{(U-2)t} * \left[x_d - 0.0238 \sqrt{\frac{TLx_d}{U-2}} \right] \quad (1)$$

where D_{nssm} ($x10^{-12}$ m^2/s) is the non-steady-state migration coefficient, T (°K) is the average value of the initial and final temperatures in the electrolyte solution, L (mm) is the thickness of the specimen, t (hr) is the test duration, x_d (mm) is the average value of the penetration depth, and (U-2) (Voltage) represents the potential difference between the two surfaces of the specimen. Thus the voltage of "-2" was used to compensate the overpotential effect. Some studies showed that the value of overpotential changes with the voltage and time applied and the electrode materials used in the test. McGrath and

Hooton [8] proposed a new conduction setup with two reference electrodes and found that the overpotential tends to increase with applied voltage. Spiesz and Brouwers [10] measured the polarized potential on the stainless steel (SS) and MMO-TiO2 electrodes under the 30V applied voltage. It was found that the magnitude of the overpotential change with the current was in the range from 1.8V to 2.2V for SS electrodes and 1.5V~1.8V for MMO-TiO2 electrodes. These experimental results indicate that the potentials at concrete surfaces vary with time due to the gradual decrease of current during the RCM test [10-12].

In the ICCP system, an impressed current or voltage is applied between the rebar in concrete and the auxiliary anode placed at concrete surface. At the rebar cathode, the potential would be more negative when low current density is applied [13]. The 100-mV potential shift, reflecting the change of overpotential, at cathode given by British Standard 7361-1 is widely used to evaluate the protective effect of ICCP system [2, 13-16]. Oleiwi et al. [2] found that the cathodic potential shift changes with the time, degree of chloride contamination, and applied current through the experiments. Hassanein et al. [17] and Muehlenkamp et al. [15] proposed a series of 2-D models to simulate the ICCP system, in which the cathodic boundary conditions are time-dependent. They found that cathodic Tafel slope, external voltage and pore saturation have a significant impact on the value of potential shift at cathode. It should be noted that the electro-potential conditions at anodic boundaries were not time varying, implying that the polarization of anode was not taken into account in these models. However, Helm et al. [18] reported that the maximum difference in cathodic overpotential calculated between using the constant and time-dependent anodic boundaries is about 50 mV. This indicates that, although the anode is placed outside of concrete, the polarization of that cannot be ignored in the modelling of ICCP.

Meanwhile, apart from the externally applied potential, the different mobilities of different ionic species also lead to an internal electric field, which in turn affects the ingress process of chloride ions [11, 19, 20]. To examine the multi-species interactions

in ionic transport process, finite element models have been developed based on Poisson-Nernst-Plank (PNP) equations. Samson et al. [21, 22], Truc et al. [23], Krabbenhoft et al. [24], Marriaga et al. [19], Johannesson et al. [25, 26], Paz-Garcia et al. [27], and Guo et al. [12] considered the cement/concrete as a homogenous medium and described the concentration profiles of each species and the distribution of electric field by using multi-species transport models. A series of multi-phases and multi-species models have been also implemented to reflect the heterogenous nature of concrete. Liu et al. [28-30] established 2-D multi-species and multi-phase models to investigate the effects of both aggregate shape and volume fraction on the penetration of chloride ions. Abyaneh et al. [31] conducted a series of 3-D models to study the effect of aggregate size and volume fraction and claimed that the penetration profiles slightly increase with the size distribution of aggregates. Li et al. [32] proposed a double-porosity RCM model to calculate the concentration profiles of chloride, in which the ionic diffusivity in the big pores is different from that in the small pores. Similarly, in Yang's numerical model, the heterogenous of concrete is also considered by alternating the pore structure parameters, including the pore size, tortuosity and constrictivity [33]. Unfortunately, the boundary conditions employed in these models, especially for the electric potential boundaries, are generally assumed not time dependent.

The above literature review shows that the time-varying overpotential caused by the polarization of electrodes has not been discussed in existing multi-species transport models. This paper presents a series of 2-D numerical models to describe the combination process of the mass transport in concrete and the polarization at electrode-electrolyte interfaces. Both the multi-species coupling and non-equilibrium binding of ionic species are involved in the mass transport process. The time-varying overpotential is calculated by using Tafel equations, which is used to reset the electric boundaries at each time increment step. The temporal and spatial distributions of the concentrations of chloride, hydroxyl, potassium, and sodium ions are presented. The effects of externally applied voltage, Tafel slope, exchange current density and initial conditions of concrete are also examined in this study. Findings from presented overpotential

models shed fresh light on the interaction between the chloride penetration and polarization during the RCM test.

2. Basic theory of modelling

2.1 Multi-species transport in saturated concrete

Under the action of an external electric field, the ions in a saturated concrete can transport through the diffusion caused due to concentration gradient and the migration caused due to electro-potential gradient. Therefore, the flux of each ionic species, J_i, during a migration test can be expressed as Nernst-Plank equation:

$$J_i=-D_i\nabla C_i-D_iC_i\frac{z_iF}{RT}\nabla\emptyset \qquad i=1,2,...n \tag{2}$$

where D_i, C_i, and z_i are the diffusion coefficient in pore solution, concentration, and charge number of *i-th* ionic species, respectively, F is the Faraday constant (96500 C/mol), R is the gas constant (8.314 J/(mol·K)), T is the absolute temperature (K), and $\emptyset$ is the electrostatic potential (V).

The mass conservation equation for each ionic species is expressed as:

$$\frac{\partial C_i}{\partial t}+\nabla\cdot J_i=R_i \tag{3}$$

where t is the time and R_i represents the adsorption/desorption between pore solution and the hydration products. Substituting Eq. (2) into (3) leads to:

$$\frac{\partial C_i}{\partial t}=D_i\nabla^2C_i+D_i\frac{z_iF}{RT}\nabla(C_i\nabla\emptyset)+R_i \qquad i=1,2,3,...n \tag{4}$$

Eq. (4) must be solved simultaneously with the governing equation of electrostatic potential gradient $\nabla\emptyset$. The electrostatic potential gradient is comprised of two parts: the externally applied voltage and the internal electric field caused by the different mobility of different ionic species in the pore solution. To describe the coupling effects of the two electric fields, the following Poisson equation is normally adopted for modelling multi-species transport in concrete:

$$\nabla^2\emptyset=-\frac{F}{\varepsilon_0\varepsilon_r}\sum_{i=1}^{n}z_iC_i \tag{5}$$

where ε_0=8.854×10^{-12} C/(V·m) is the permittivity of a vacuum and ε_r=78.3 is the

relative permittivity of water at temperature 298K.

2.2 Time-varying overpotential at the electrode-electrolyte interfaces

During the electrochemical process, the oxygen reduction and hydrogen evolution reactions (ORR and HER) at cathode and oxygen evolution reaction (OER) and iron corrosion at anode can be described as [33, 34]:

At Cathode: $2H_2O + O_2 + 4e^- = 4OH^-$ (6)

$2H_2O + 2e^- = 2OH^- + H_2$ (7)

At Anode: $4OH^- - 4e^- = 2H_2O + O_2$ (8)

$2H_2O - 4e^- = 4H^+ + O_2$ (9)

$Fe - 2e^- = Fe^{2+}$ (10)

The polarization of electrodes includes three parts: activation polarization caused by the accumulation of non-reagent products from electrochemical reactions, concentration polarization induced by the depletion of reagents near the electrodes, and ohmic polarization [35]. Hence, the potential difference between the electrode and concrete surface can be presented as:

$$\eta = \eta_{act} + \eta_{ohm} + \eta_{conc} \tag{11}$$

where η, η_{act}, η_{ohm} and η_{conc} are the overall, activation, ohmic and concentration overpotential at the electrode-electrolyte interfaces, respectively.

The activation overpotential, η_{act}, can be determined by using Tafel equation as follows [36]:

$$\eta_{act} = \beta \log \frac{I}{i_0} \tag{12}$$

where β is the Tafel slope, i_0 is the exchange current density, and I is the current density at electrode. β and i_0 are dependent on the type of chemical reactions, the concentration of electrolyte, the material of electrode, temperature, etc. The value range of Tafel parameters for three main reactions during RCM, HER and OER, is summarized in Table 1.

Table 1 Summation of Tafel parameters for three main reactions.

Tafel parameters	Notation	ORR	HER	OER
Tafel Slope (mV/decade)	β	100~490 [36-41]	30~208 [37, 42, 43]	24~199 [44]
Exchange current density ($\times 10^{-7}$A/m^2)	i_0	62.5~2000 [36-41]	1400~10000 [43]	6~1000 [45]

The ohmic overpotential at the electrode-electrolyte interfaces is due to the resistance of electrode's line segment, which is very small and thus can be ignored [35]. The value of concentration overpotential is described as [35]:

$$\eta_{conc}=\frac{RT}{nF}\ ln(1-\frac{I}{i_L}) \tag{13}$$

where i_L is the limiting current density and n is the number of transferred electrons in reactions.

Therefore, the overall overpotentials at electrode-electrolyte interfaces can be calculated by the following equations:

$$\eta_a=\beta_a\ log\frac{I_a}{i_{a,0}}+\frac{RT}{nF}\ ln(1-\frac{I_a}{i_L}) \tag{14}$$

$$\eta_c=\beta_c\ log\frac{I_c}{i_{c,0}}+\frac{RT}{nF}\ ln(1-\frac{I_c}{i_L}) \tag{15}$$

where, η_a, η_c, β_a, β_c, $i_{a,0}$ and $i_{c,0}$ represent the overpotential, Tafel slope and exchange current density at anode and cathode, respectively, I_a and I_c are the current density flow into/out from the concrete sample, which, with the assumption of current conservation, can be determined as follows:

$$I_c=F\sum_{i=1}^{n}z_iJ_i\ \Big|_{x=0} \tag{16}$$

$$I_a=F\sum_{i=1}^{n}z_iJ_i\ \Big|_{x=L} \tag{17}$$

Due to the polarization of electrodes, the anode becomes more positive, whereas the cathode tends to be more negative. Hence, the electric potential at the cathodic (Φ_{sc}) and anodic (Φ_{sa}) surface of concrete can be reset as:

$$\Phi_{sc}=\Phi_c+\eta_c \tag{18}$$

$$\Phi_{sa}=\Phi_a-\eta_a \tag{19}$$

Thus, the potential across the concrete specimen can be expressed as:

$$\Delta\Phi_s=\Phi_{sa}-\Phi_{sc}=\Phi_a-\Phi_c-\eta_a-\eta_c=\Delta\Phi-(\eta_a+\eta_c) \quad (20)$$

where Φ_a and Φ_c represent the electric potential at anode and cathode, respectively. $\Delta\Phi$ is the externally applied voltage. From Eqs. (14)-(20), it can be noticed that the polarization will influence the actual potential throughout the concrete specimen and thus affect the ionic transport process in the specimen. In turn, the ions transport in concrete can also influence the overpotential value.

2.3 Non-equilibrium chloride binding involved in ionic transport

There is a liquid-solid interface between pore solution and hydration products in concrete [46]. The chloride adsorption can be divided into two processes: firstly, chloride ions transfer from pore solution towards the liquid-solid interface, and then part of them are adsorbed into the hardened cement surface [47]. Similarly, for the desorption process, chloride ions are first released from the solid phase into the interface, and then transported into the liquid phase driven by the concentration gradient between two phases. This means that a certain period is needed to overcome the resistance of the liquid-solid interface and achieve the equilibrium between the free chloride concentration in liquid phase and bound chloride concentration in solid phase. Tang and Theissing found that it requires 7~14 days to bring the absorption into equilibrium in hardened concrete [48, 49]. Due to the duration of chloride migration tests that is usually less than two days, the equilibrium between free and bound chlorides cannot be reached in such a short period. The previous studies reported that the ingress depth of chlorides will be underestimated with considering the equilibrium binding in RCM tests [50, 51]. Hence, Spiesz et al. [47] and Li et al. [32] introduced a mass transfer item to calculate the non-equilibrium binding of chlorides in the single species transport models. However, the previous studies reported that the existence of other ions, OH^-, K^+, Na^+, can also influence the binding balance by the multi-species interactions and the adsorption of themselves in CSH [12, 52]. In the present work, it is assumed that the binding of sodium, potassium, and hydroxyl ions is in proportion to

the bound chloride ions. Therefore, the non-equilibrium binding between the liquid and solid phases can be expressed as:

$$R_i = p_i \ k_s \ (C_{cl^-} - C_s) \qquad i=1,2,...n \tag{21}$$

where, R_i and p_i are the mass transfer rate and the binding proportion coefficient of *i-th* ionic species, respectively. To keep the charge balance in the liquid-solid interface, the binding proportion coefficient of Cl^-, OH^-, K^+, Na^+ can be simplified as 1, 1/3, 2/3, 2/3, respectively. k_s is the adsorption/desorption rate of chloride, C_{cl^-} is the free chloride concentration in pore solution, C_s is the chloride concentration in the liquid-solid interphase. Assuming the absorption and desorption of chloride take place instantaneously, C_s can be determined by the Langmuir isotherm:

$$S_{cl^-} = \frac{\alpha C_s}{1+\beta C_s} \tag{22}$$

where, α and β are the binding constants, which can be determined by a series of experiments, S_{cl^-} is the bound chloride in hardened cement. Submitting Eq. (22) into (21), it yields:

$$R_i = p_i \ k_s \ \left(C_{cl^-} - \frac{S_{cl^-}}{\alpha - \beta S_{cl^-}}\right) \qquad i=1,2,...n \tag{23}$$

Hence, this non-equilibrium binding process can be described as: when the chloride concentration in the interface is lower than it in pore solution, chloride ions continually transfer into the interphase, and the concentration of bound chloride in cement will increase. When the concentration of chloride ions in the interface is higher than in pore solution, they are transported from interface to liquid phase. Then, bound chloride will be released to keep the equilibrium between liquid-solid interface and solid phase. And the bound concentrations of sodium, potassium, and hydroxyl ions decrease or increase accordingly. Hence, the multi-species mass transportation for liquid and solid phase can be evaluated by the following equations:

$$\frac{\partial C_i}{\partial t} = D_i \nabla^2 C_i + D_i \frac{z_i F}{RT} \nabla (C_i \nabla \emptyset) - p_i \ k_s \ (C_{cl^-} - \frac{S_{cl^-}}{\alpha - \beta S_{cl^-}}) \qquad i=1,2,...n \tag{24}$$

$$\frac{\partial S_i}{\partial t} = p_i k_s \ \left(C_{cl^-} - \frac{S_{cl^-}}{\alpha - \beta S_{cl^-}}\right) \qquad i=1,2,...n \tag{25}$$

where S_i is the bound concentration of *i-th* ionic species.

3. Numerical modelling

3.1 Geometric model and input parameters

A series of multi-phases models are developed to obtain the temporal and spatial distributions of ionic species in the concrete and the overpotential at electrodes for the simulation of RCM tests. As shown in Figure 2, a two-dimensional geometry of 50 mm × 50 mm representing an axially symmetrical concrete specimen is built, in which the randomly distributed circles represent the impermeable aggregates and the dark areas stand for the cement pastes. Aggregate is the key component to concrete. Both the volume fraction and size distribution of aggregates can affect the chloride resistance of the mixed concrete. In existing multi-phase models, the size distribution of aggregates is usually in the range of 2~20 mm [29, 53, 54]. Nevertheless, Abyaneh et al. [31] found that the aggregates with a diameter of 0.15~2 mm have a significant impact on the chloride resistance of concrete. Therefore, the diameters of aggregates used in this study are chosen from 0.15 mm to 20 mm. The particle size distribution of aggregates follows Fuller's grading curve, and the volume fraction of aggregates (Va) is 0.5. Additionally, to equilibrate the relationship among the accuracy, computational time and convergence of numerical solutions, the size of free triangular meshes are adaptively adjusted [55]. Due to the extremely fine aggregates that are used in the geometrical model, the minimum size of meshed elements has been adjusted to be 3.75×10^{-6} m, for which a total of 202500 elements are used in the domain.

As shown in Figure 1, the cathodic and anodic surfaces of the cement-based material are exposed to the electrolyte solutions of 520 mol/m^3 NaCl and 300 mol/m^3 NaOH, respectively. As the volume of the electrolyte solutions is much larger than that of the pore solution in the specimen, the concentrations of the NaCl and NaOH solutions on the two sides of the specimen are assumed as constants. Four ionic species (potassium, sodium, chloride, and hydroxyl ions) are considered, and an external stable voltage is applied between the two surfaces. Because of their low concentrations in the concrete

pore solution, the calcium and sulphate ions are not considered in the simulation. The diffusion coefficients, initial and boundary conditions of ionic species, Tafel parameters, and binding constants used in the study are given in Table 2.

Table 2 Input parameters used in numerical simulations.

Parameter	Notation	Value in base case	Values in parametric studies
Water/cement ratio	w/c	0.35	0.35
Porosity (%)	φ	11.3	11.3
Aggregate volume fraction	V_a	0.5	0.5
Diffusion coefficient	K^+	1.96 [11]	1.96 [11]
($\times 10^{-11}$ m^2/s)	Na^+	1.33 [11]	1.33 [11]
	Cl^-	2.03 [11]	2.03 [11]
	OH^-	5.26 [11]	5.26 [11]
Initial concentration	K^+	200	50 and 400
(mol/m^3)	Na^+	100	25 and 200
	Cl^-	0	0
	OH^-	300	75 and 600
Binding constants	α	1.40 [32]	1.40 [32]
	β	0.0008 (m^3/mol) [32]	0.0008 (m^3/mol) [32]
Adsorption/desorption rate	k_s	5.0×10^{-5} (1/s)	5.0×10^{-5} (1/s)
Tafel parameters	β_c	180 (mV/decade)	100 and 280
	$i_{c,0}$	10 ($\times10^{-6}$A/m^2)	6 and 100
	β_a	120 (mV/decade)	60 and 200
	$i_{a,0}$	10 ($\times10^{-7}$A/m^2)	6 and 50
Voltage applied (V)	$\Delta\Phi$	24	8 and 16
Limiting current density	i_L	100 (A/m^2) [56]	100 (A/m^2) [56]

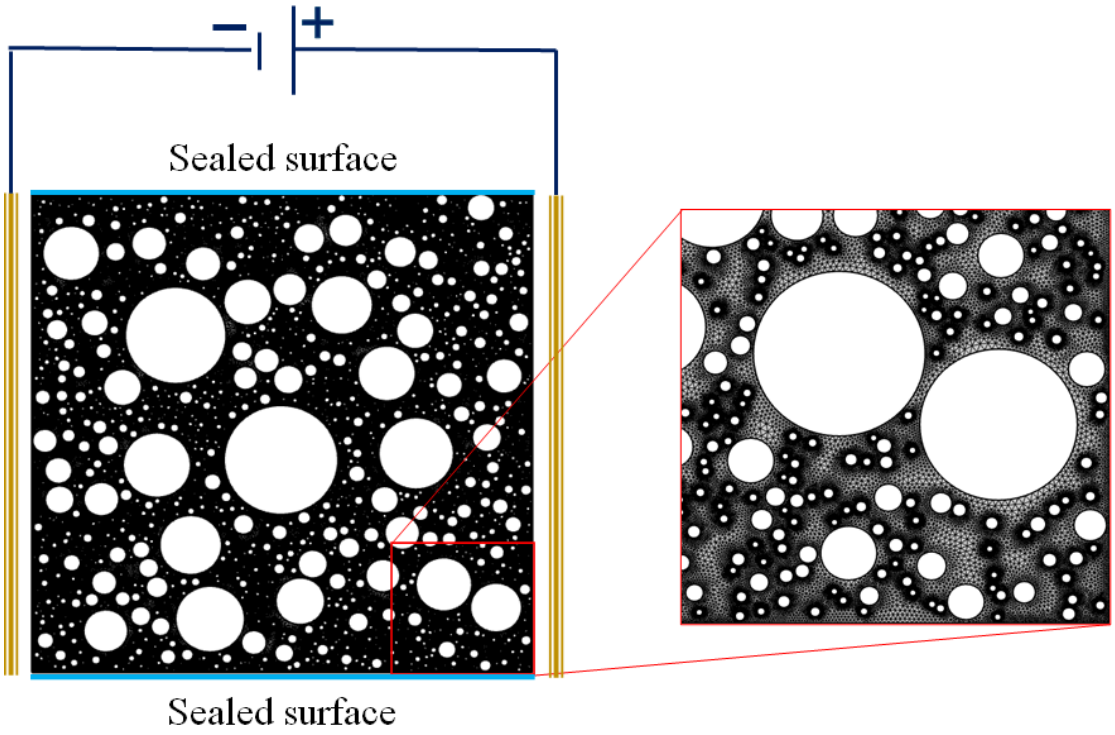

Figure 2 The geometric model and corresponding mesh used in numerical simulations (Cathode and anode are assumed to attach to the left and right sides of the concrete domain, whereas the top and bottom lines of the domain are assumed to be sealed)

3.2 Solution procedure

In the present numerical simulation models, both the mass transport and polarizing processes are considered. The former is applied to express the multi-species transport in the pore solution with adsorption/desorption of ions between liquid and solid phases. The latter is adopted to obtain the real time-varying electric boundaries at cathodic and anodic interfaces. Herein, these two processes are jointly solved by using a sequential non-iterative algorithm (SNIA), which is implemented in COMSOL. In the SNIA the potential boundaries are updated at each time increment step so that an accurate and unique solution can be reached. As shown in Figure 3, firstly, the concentration of each species in concrete, overpotentials and potential boundaries at anodic and cathodic interfaces are initialized as C_i^0, η_a^0, η_c^0, 0, U, respectively. Using the values of C_i^n, η_a^n, η_c^n obtained from previous step, the uncorrected concentrations $C_i^{n+1'}$ can be

solved by Eqs. (5), (24) and (25). After calculating the overpotential at electrodes based on Eqs. (14) and (15), the cathodic and anodic boundary conditions are reset as η_a^{n+1}, U-η_c^{n+1}, respectively. Finally, the corrected concentrations C_i^{n+1} is updated and used in the next step of calculation. All governing equations are solved at each time increment by using the finite element method built in COMSOL. Based on this, the interaction between ionic transport and polarization and the influences of heterogenous of concrete, applied voltage, Tafel parameters and initial ionic species concentration on the ionic transport in concrete are investigated in following sections.

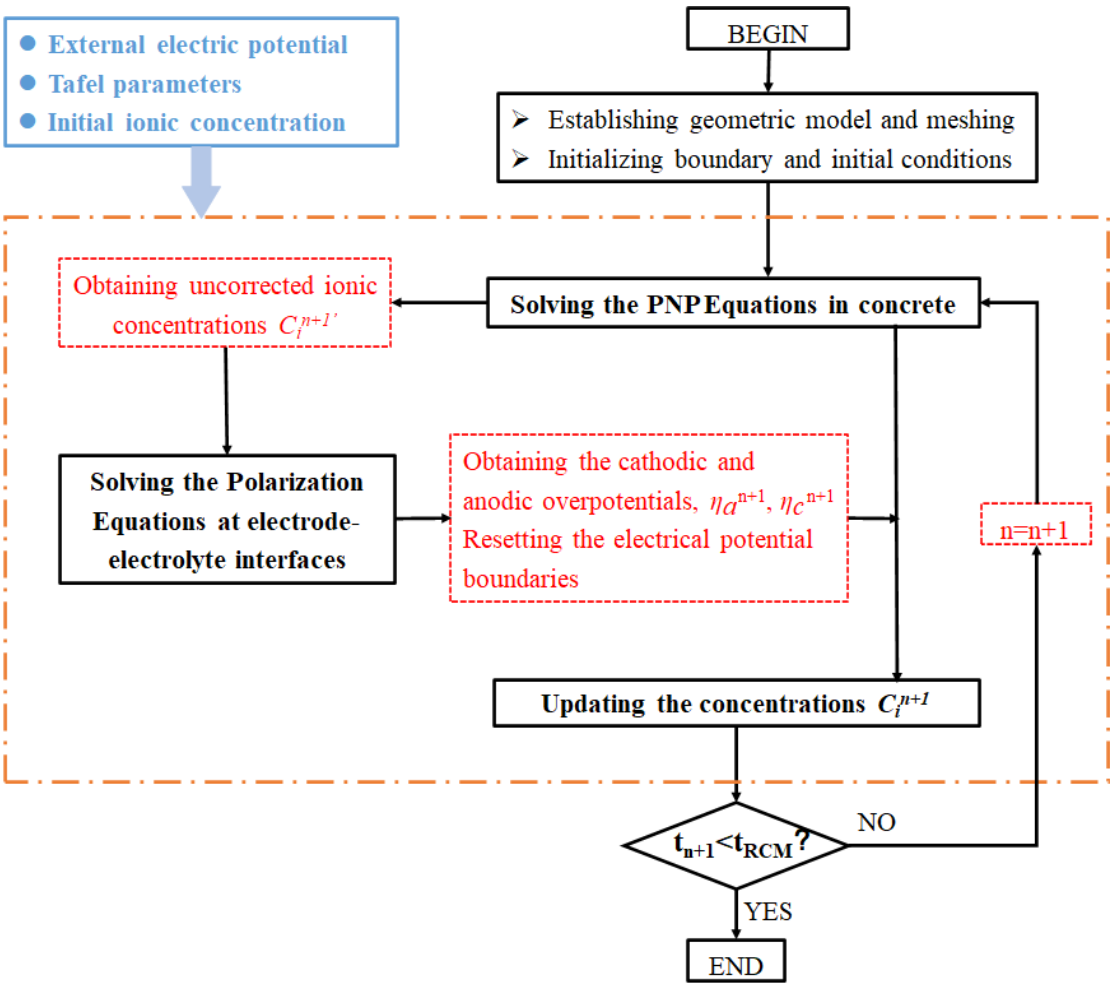

Figure 3 Solution procedure used in overpotential model

4. Benchmark

This section aims at demonstrating the reliability of the proposed models and examining

the effect of overpotential on ionic transport in migration tests. Firstly, some details of presented model are adjusted to be consistent with two existing chloride migration tests conducted by Jiang et al. [57] and Castellote et al. [58], respectively. As shown in Table 3, these adjusted parameters include the size of cement/concrete specimen, the water/cement ratio, the corresponding binding constants (α and β), the initial concentration in pore solution, the external DC voltage, the volume fraction of aggregates, the concentration of electrolyte and the test time. Note that calcium and sulfate ions are ignored due to their low concentrations in the pore solution. Then the initial concentrations of other species are adjusted according to the condition of electroneutrality.

Table 3 Input parameters in benchmarked models.

Parameters	Notation	Jiang's expt.	Castellote's expt.	Note
Size of specimen (mm×mm)	-	50×100	75×150	[57, 58]
Water/cement ratio	*w/c*	0.5	0.4	[57, 58]
Binding constants	α	1.686	0.87	Taken from [59] and recomputed
	β	0.0099	0.0047	for concentration unit (m^3/mol).
Initial concentration	K^+	600	700	The values in Castellote's expt.
(mol/m^3)	Na^+	202	200	are estimated from the chemical
	Cl^-	0	0	analysis of cement. [57, 58]
	OH^-	802	900	
External DC power (V)	$\Delta\Phi$	30	12	[57, 58]
Aggregate volume fraction	V_a	0.75	0	Estimated from aggregates dosage used in experiment.
Anolyte (mol/m^3)	*NaOH*	300	300	[57, 58]
Catholyte (mol/m^3)	*NaCl*	500	500	[57, 58]
Duration	-	28 Days	36 Hours	[57, 58]

The penetration depth of chloride in the chloride migration test is the key indicator to calculate the chloride migration coefficient and for the prediction of the service life of concrete structures. As demonstrated in NT Build 492, the threshold for detected chloride by colorimetric method is approximately 70 mol/m^3 [7]. Therefore, the effective chloride penetration depth for both experimental and numerical results are

determined by using this value. Figure 4 elaborated the comparison between experiments and simulations with and without considering the effect of overpotential. It can be found that the verification results from the overpotential models are demonstrated. The simulation results of Jiang's experiment are smooth curves, and the result with overpotential fits well with the results from cement specimens. However, due to the use of aggregates phase in modelling of Castellote's experiment, the penetration depth profiles have fluctuating shapes, in which the difference in chloride penetration depth between the numerical and experimental results ranges from 2.7~4.1 mm at 7 days and 2.5~3.1 mm at 28 days, respectively. The figure also shows that, in terms of both the experimental data, the non-overpotential models overestimate the chloride permeability. Therefore, the electrode polarizing process should be included when simulating chloride migration test.

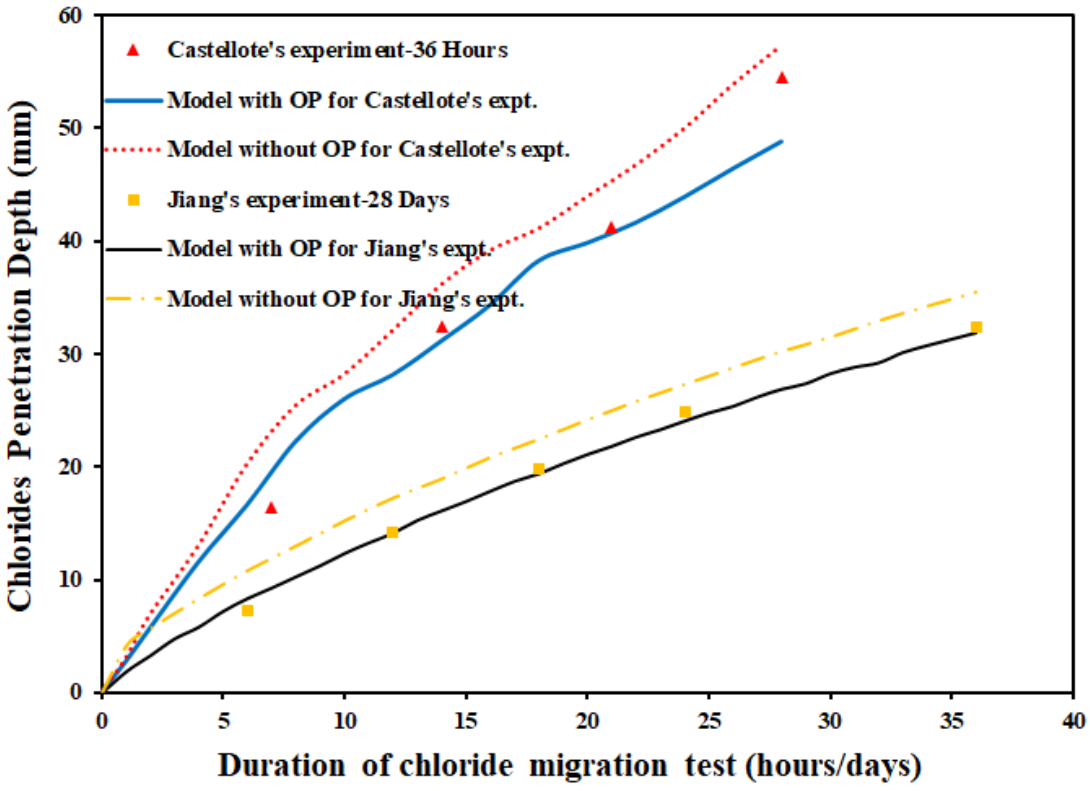

Figure 4 The comparison between experimental and numerical simulation results.

5. Results and discussion

5.1 External applied voltage

The externally applied electric field is the dominant driving force for ionic transport in chloride migration tests. Hence, to reflect the effect of externally applied voltage on both the ionic concentration distribution and polarization process, three external applied voltages, 8V, 16V and 24V, are used in the simulations, whereas all other input parameters are assumed to be the same as those given in the base case of Table 2.

Figure 5 shows that total overpotential in the 24V-model decreases from 2.26V to 2.14V over the 24 hrs testing time, due to the current density flow through the concrete gradually dropping during RCM test (see Figure 6). According to Eq. (20), the actual potential difference throughout the whole specimens drops approximately 8.9~9.4 % than that applied on electrodes, which means that the actual driving force provided by the electrostatic potential gradient would be slightly small. Hence, the penetration depth of chloride ions is smaller in the models involving the polarization process than that in the non-overpotential models, as shown in Figure 7. The red line in each model represents the effective penetration depth, where the concentration of chloride ions is 70 mol/m^3 [6]. It can be observed that the chloride ions gradually ingress into concrete under the action of externally applied electric field. In order to describe the influence of overpotential more intuitively, the concentration profiles of chloride ions are replotted in Figure 8, where the profiles of hydroxyl, sodium, and potassium ions are also included. It is interesting to note that, although the overpotential decreases over time, the difference in chloride penetration depth between the overpotential and non-overpotential models becomes increasingly apparent. Meanwhile, due to the multi-species coupling effect, the concentration distributions of K^+, Na^+, and OH^- ions change correspondingly. Moreover, the influence of the overpotential on the transport of OH^- and K^+ ions is more evident than its influence on Na^+ ions. There are two possible reasons for this phenomenon. One is due to the large diffusion coefficients of OH^- and K^+ ions. The other is owing to the fact that the anodic electrolyte NaOH solution

provides sufficient Na^+ ions moving through the concrete specimens.

It also can be seen from Figure 5 that the overpotential slightly increases with the increase of externally applied voltage. This agrees with the results from McGrath's experiment [58], in which the overpotential ranged from 1.91 to 2.36V when the externally applied potential increased from 6V to 30V. Figure 6 shows that the current density flow through the concrete increases with the increased external voltage, which enables stronger polarization occurs at electrode-electrolyte interfaces. The overpotential, in turn, affects the concentration distribution of each ionic species in pore solution and finally changes the current density flow through concrete, as shown in Figures 6 and 9. This implies that there is an interaction between ionic transport and polarization processes. In addition, the difference of overpotential between 8V-, 16V- and 24V-models and the value of overpotential show a decreasing trend with time. This is because the discrepancies of current density between 8V-, 16V- and 24V-models decrease quickly during the first 12 hours (see Figure 6), which confirms the results from Spiesz's experiments [10]. Figure 9 shows the concentration profiles of chloride ions obtained from the overpotential and non-overpotential models with different external voltages. It can be observed that the larger the externally applied voltage, the deeper the chloride ingress depth in concrete. This is because the velocity and the total amount of species passing through the concrete are greater under the higher externally applied driving force. Moreover, the impact of overpotential on chloride ingress tends to increase with the decline of the external voltage. This tendency is consistent with the results in the benchmark. The decrement of ingress depth caused by polarization under 8V applied voltage is approximately 1.5 times that under 16V applied voltage and 2.4 times that under 24V applied voltage. This means that the decline of chloride ingress not only is affected by the magnitude of overpotential but also is determined by the proportion of it to the externally applied voltage.

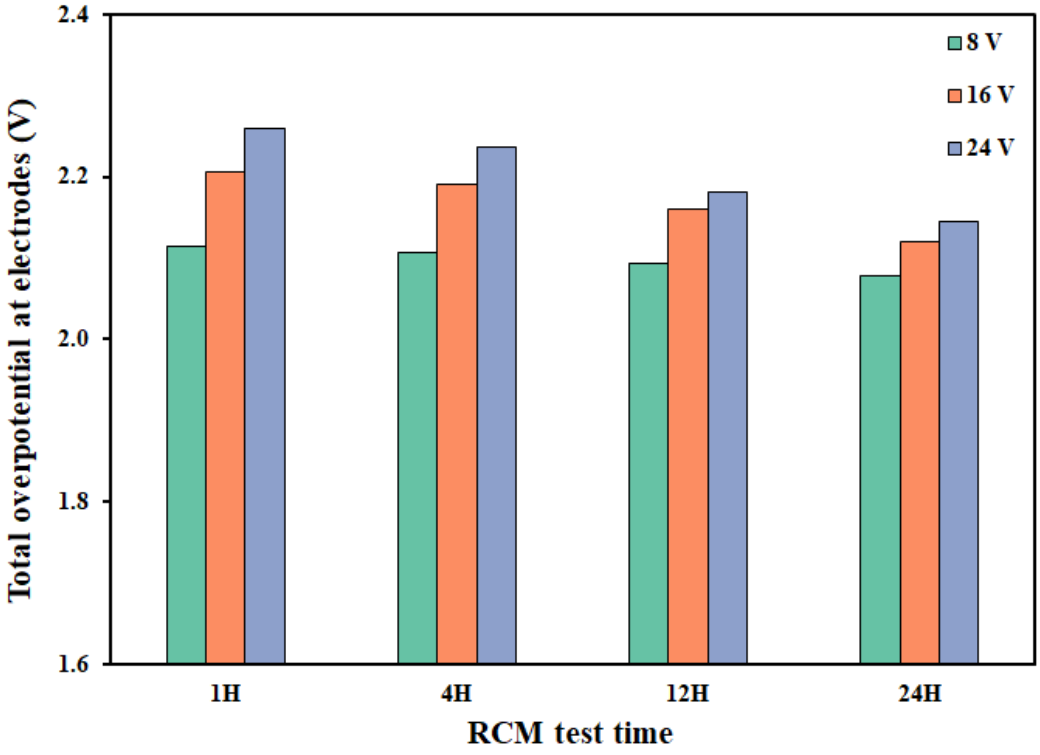

Figure 5 The values of total overpotential at anodic and cathodic interfaces, $\eta_a+\eta_c$, for models with different externally applied voltages.

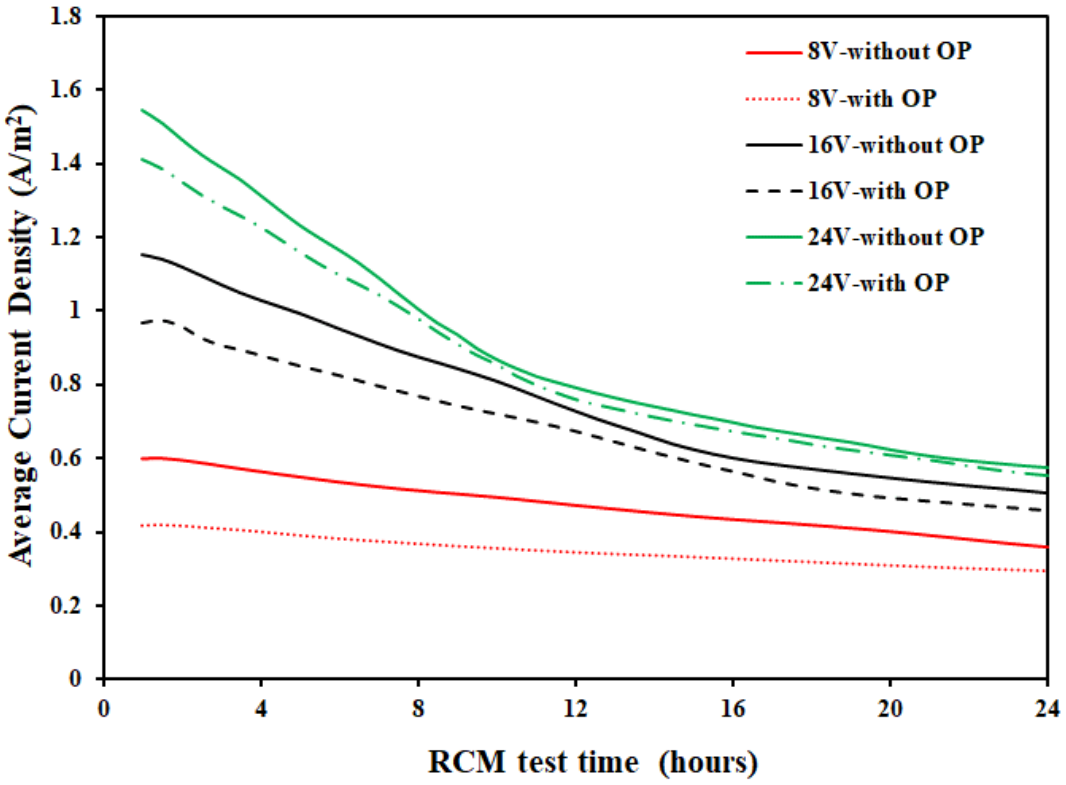

Figure 6 The average current density in the RCM models with and without considering the overpotential (OP) when three different voltages applied.

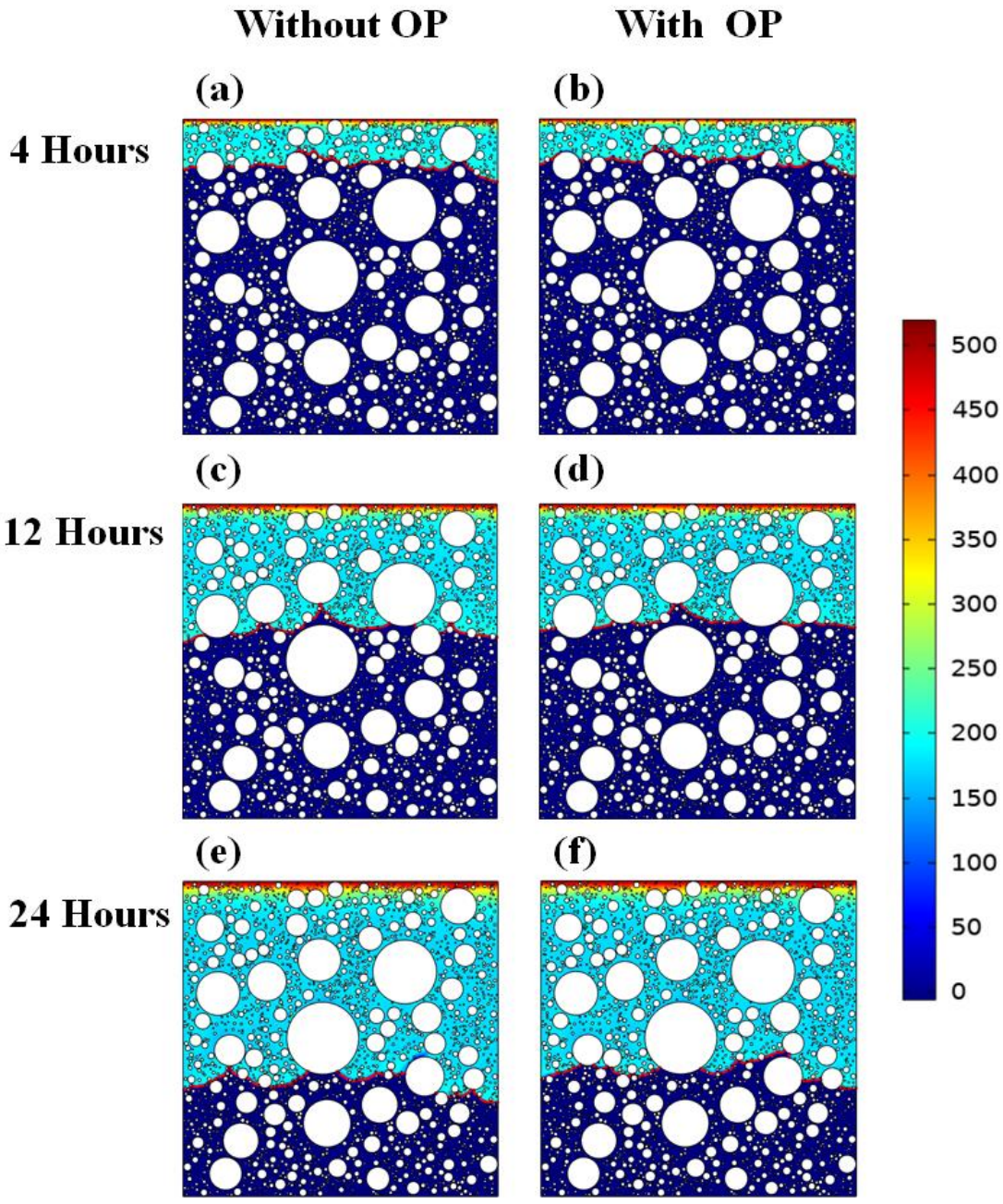

Figure 7 Chloride spatial distributions at three different times in 24V-models (mol/m^3)

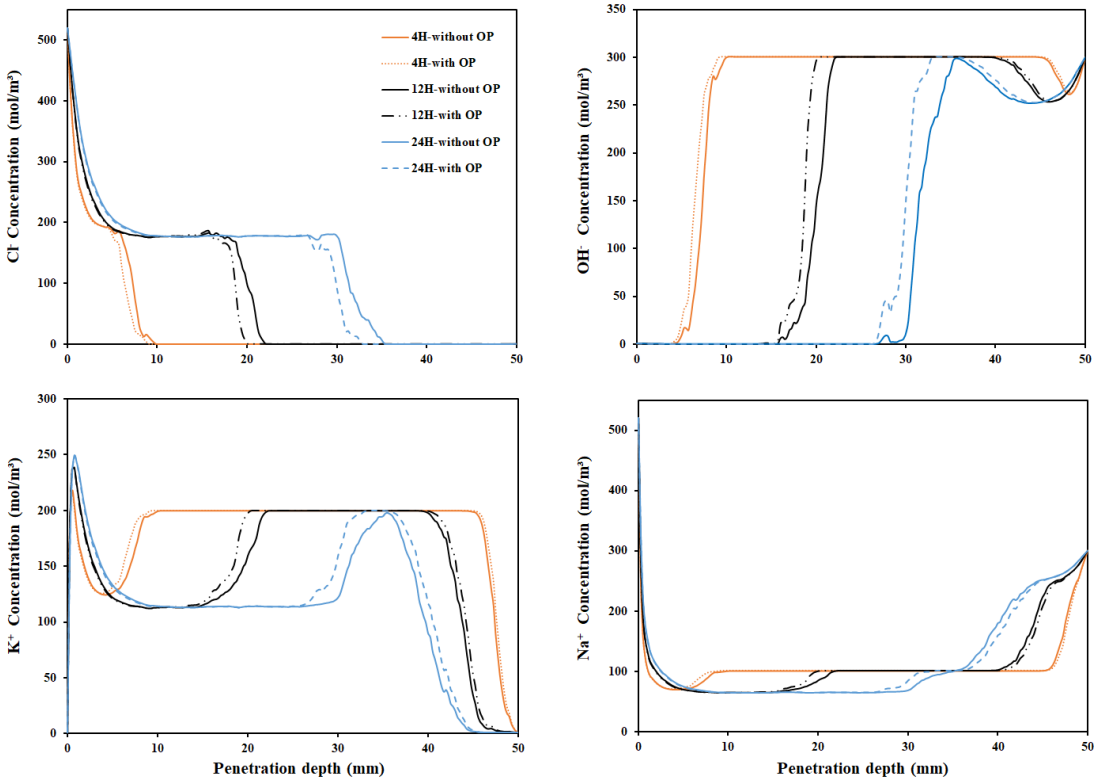

Figure 8 Concentration distribution profiles of Cl^-, OH^-, K^+, Na^+ ions in 24V-models with and without considering the overpotential (OP) at three different times.

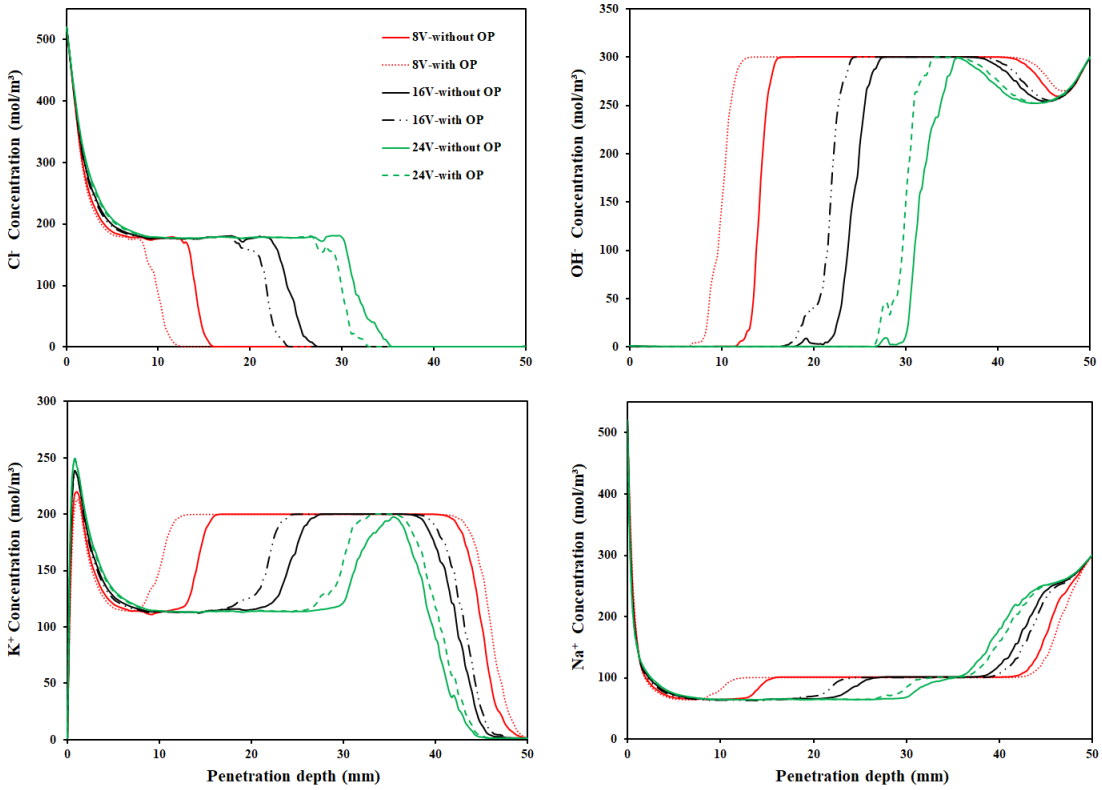

Figure 9 Concentration distribution profiles of Cl^-, OH^-, K^+, Na^+ ions in the models with and without considering the overpotential (OP) when three different voltages applied.

5.2 Tafel parameters

According to Eqs. (14) and (15), the overpotential is partly determined by the Tafel slope and exchange current density. These two Tafel parameters are dependent on the electrode material, electrolyte, electrochemical reactions, etc. Based on the main electrochemical reactions described in section 2.2 and the electrolyte used in the migration test, five sets of Tafel parameters are selected (see Table 4). The externally applied voltage is 24V. The initial concentrations of Cl^-, OH^-, K^+, and Na^+ ions are 0, 300, 200 and 100 mol/m^3, respectively.

The total overpotential in the five cases at 1 hour, 12 hours and 24 hours are plotted in Figure 10. As expected, the overpotential is proportional to the Tafel slope and inversely proportional to the exchange current density. The Tafel slope plays a vital role in the magnitude of overpotential, while the influence of exchange current density is limited. The value of overpotentials in the Highest and High cases is three times greater than that in the Lowest and Low cases. The difference of overpotential between each case is almost the same at any time. It should be noticed that the total overpotential in the Highest and High cases holds in the range of 2.65V~3.24V, which is far above the value tested/adopted in experiments and NT Build 492 [7, 8, 10]. Therefore, selecting suitable Tafel parameters in the numerical analysis of overpotential between electrodes and specimen surfaces is important. Figure 11 shows the concentration distribution profiles of each ionic species in five overpotential cases. For the purpose of comparison, the concentration profile of chloride ions in non-overpotential model is also superimposed in the figure. There are no apparent differences in terms of the ionic distribution between the Highest and High cases, or between the Lowest and Low cases. In contrast, the differences between the Low, Base and High cases are significant. In addition, a high Tafel slope can enlarge the influence of exchange current density on both the overpotential and penetration depth of chloride ions. The penetration depth of chloride ions is negatively associated with the overpotential. The lower the overpotential on electrodes, the higher the potential drop throughout the concrete specimen, hence the more the chloride ions move into concrete.

Table 4 Parametric study grid

Parameter	Highest case	High case	Base case	Low case	Lowest case
β_a (mV/decade)	200	200	120	60	60
$i_{a,0}$ (10^{-7}A/m^2)	6	50	10	50	6
β_c (mV/decade)	280	280	180	100	100
$i_{c,0}$ (10^{-6}A/m^2)	6	100	10	100	6

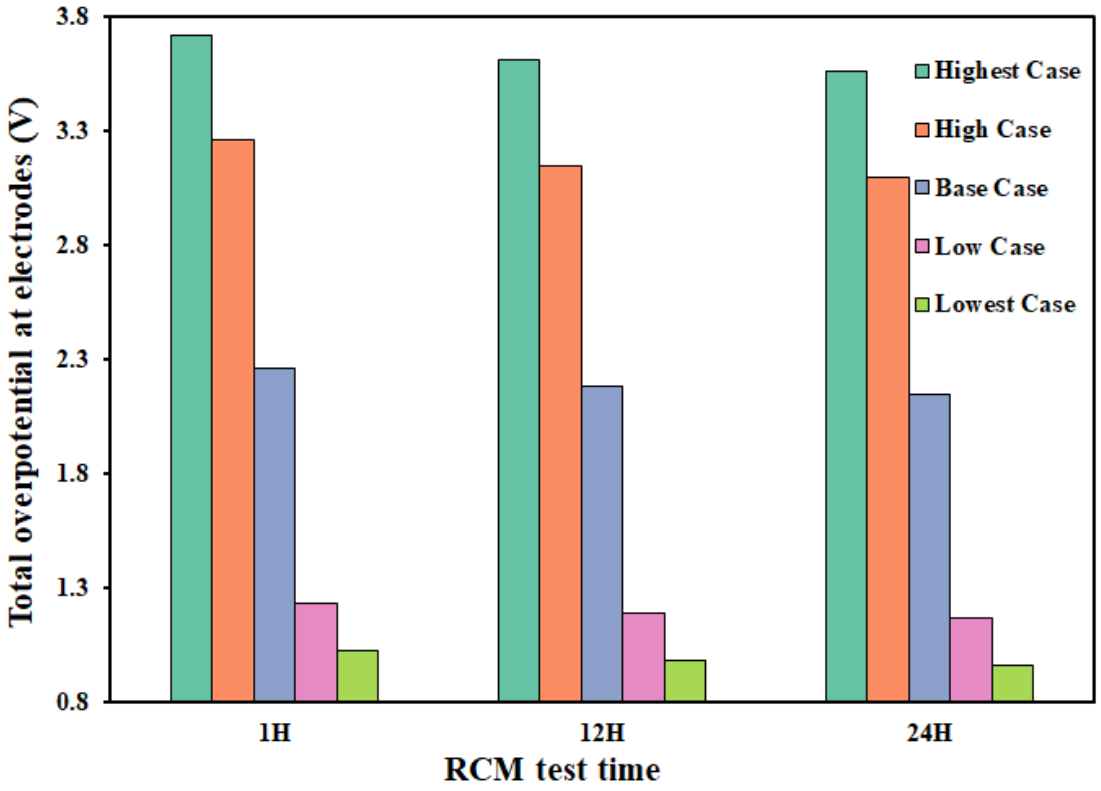

Figure 10 The values of total overpotential at anodic and cathodic interfaces, $\eta_a+\eta_c$, for models with different Tafel parameters.

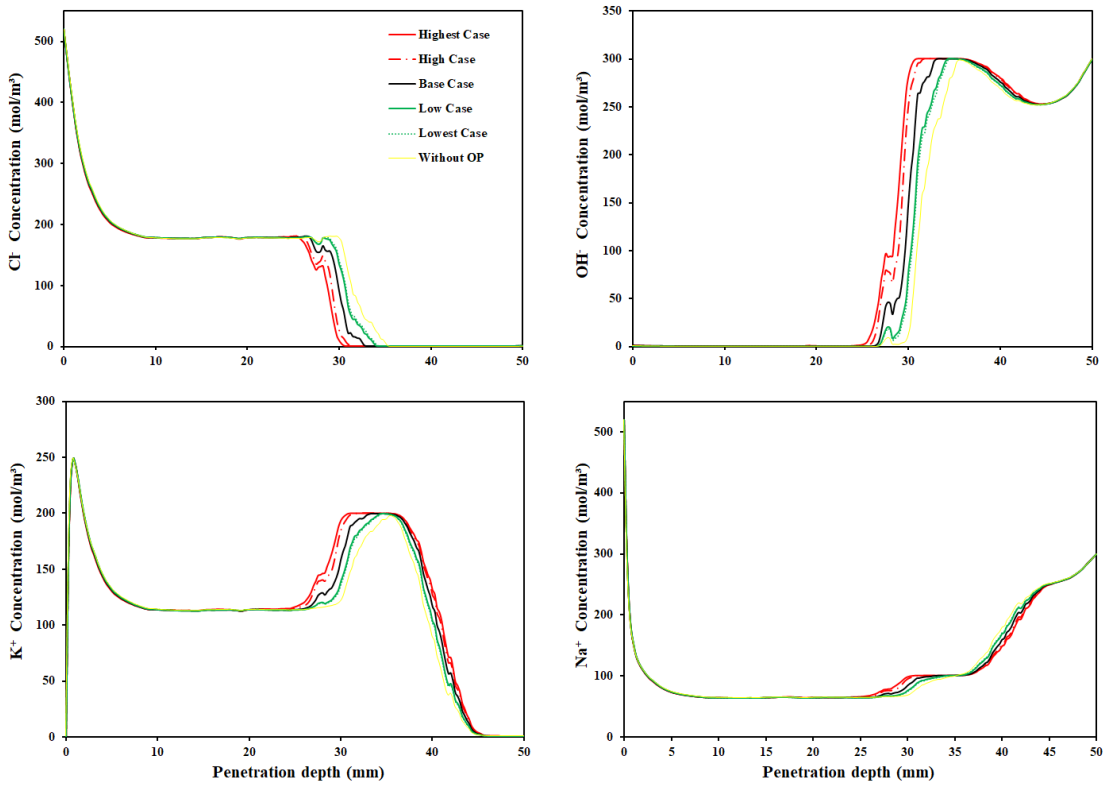

Figure 11 Concentration distribution profiles of Cl^-, OH^-, K^+, Na^+ ions in the cases with different Tafel parameters after 24-hour RCM test.

5.3 Initial concentration in the pore solution

For different types of cement, the initial concentrations of ionic species in their pore solutions may also be different, which thus can affect the flux of ionic species at concrete surfaces. According to Eqs. (16) and (17), the current density flow into/out from concrete surfaces is related to the fluxes of each species and then perhaps finally changes the polarization process at electrode-electrolyte interfaces. Herein, three different initial concentrations are used, which are given in Table 5, and other input parameters remain the same as those used in the base case in Section 5.2.

Figure 12 shows the changes of total overpotential in three different initial concentration cases. The higher initial concentration results in higher current density and thus higher overpotential (see Figures 12 and 13). A possible explanation for this might be that the higher initial concentration in pore solution can provide more ions to be exchanged into/out concrete and leads to higher ionic fluxes. It also can be found

from Figure 13 that the differences between current densities in three cases are not remarkably changed with time. Therefore, the discrepancies of overpotential between each case are almost the same over time and are in the range of 0.1V~0.2V. Figure 14 shows the concentration profiles of each ionic species in three different initial concentration models. From Figure 14, it can be observed that the effect of initial concentration on the total amount of chloride ions ingress into concrete is significant. The more the initial ionic species in pore solution, the more the chloride ions can be moved into concrete. As the initial concentration in Case 1 is low, the 70 mol/m^3 is unsuitable for use as a criterion to obtain the chloride penetration depth. In this section, the penetration depth can be determined as the depth of mid-point between the wavefront and the zero concentration point of the chloride profiles. The chloride penetration depth in Case 1, 2 and 3 without the overpotential is 32.5, 32.6 and 33 mm, respectively. This means that the penetration depth is almost independent of the initial concentration. It also can be seen that the effect of overpotential on chloride penetration depth in higher initial concentration case is more noticeable.

Table 5 Initial concentrations of Cl^-, OH^-, K^+ and Na^+ ions (mol/m^3)

	Potassium	Sodium	Chloride	Hydroxide
Case 1	50	25	0	75
Case 2	200	100	0	300
Case 3	400	200	0	600

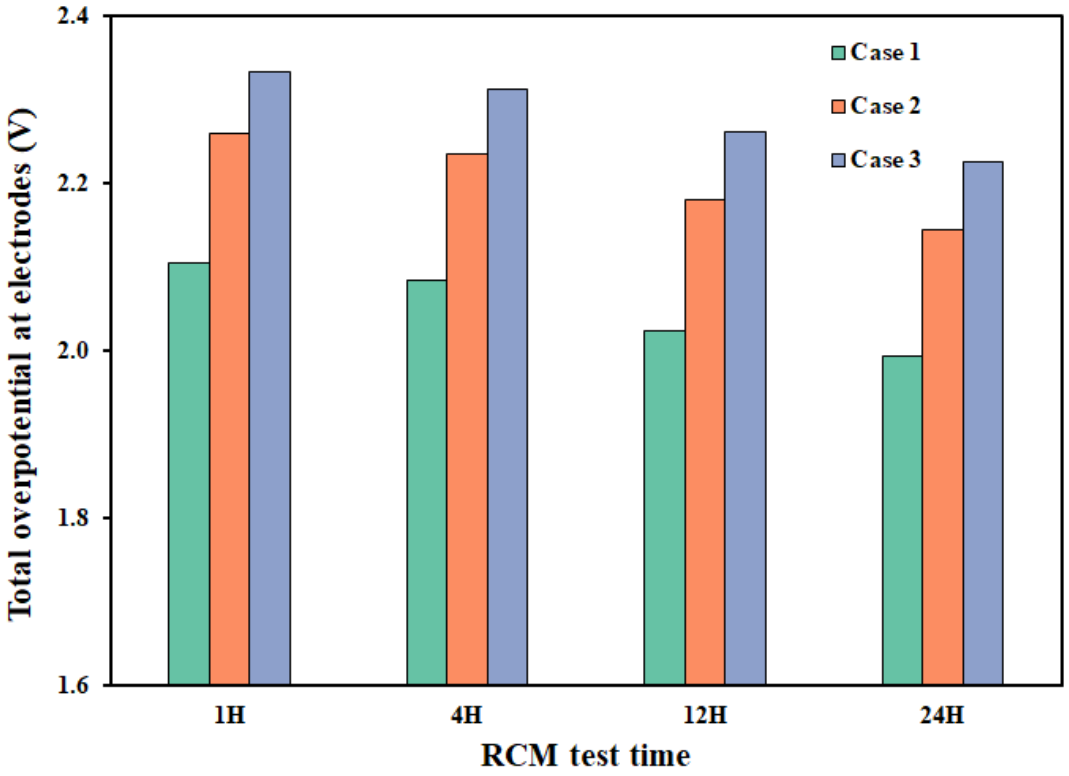

Figure 12 The values of total overpotential at anodic and cathodic interfaces, $\eta_a+\eta_c$, for models with different initial concentrations

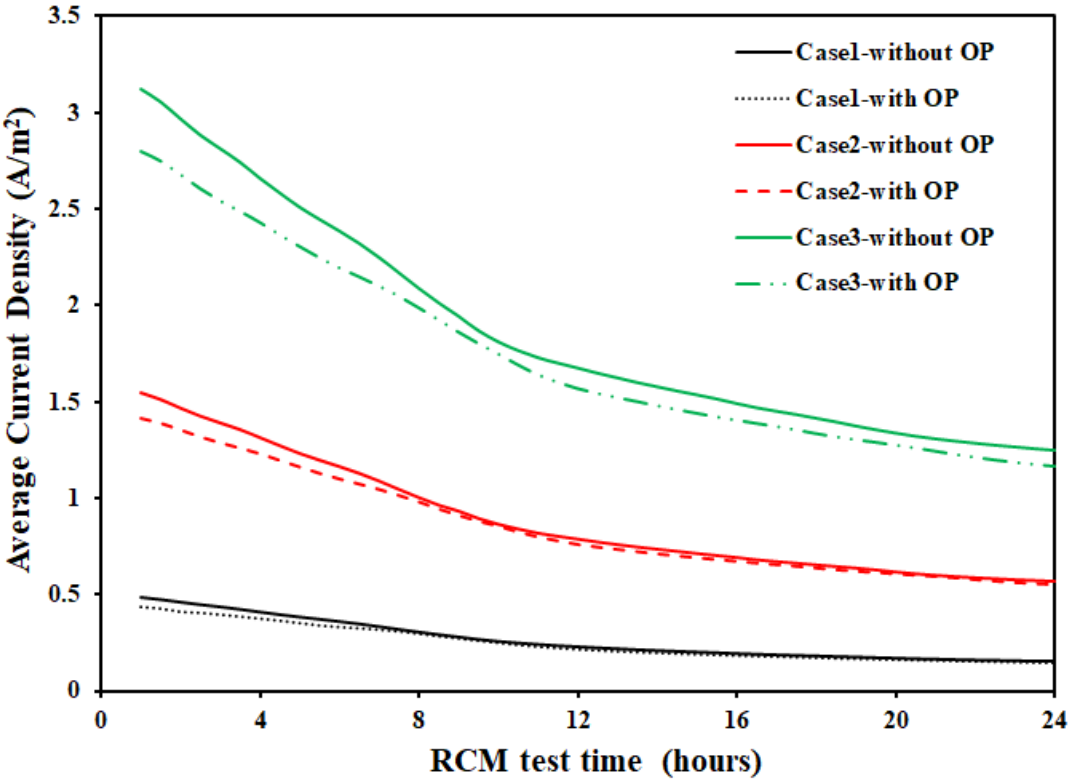

Figure 13 Figure 6 The average current density in the RCM models with and without considering the overpotential (OP) when three different initial pore concentrations applied.

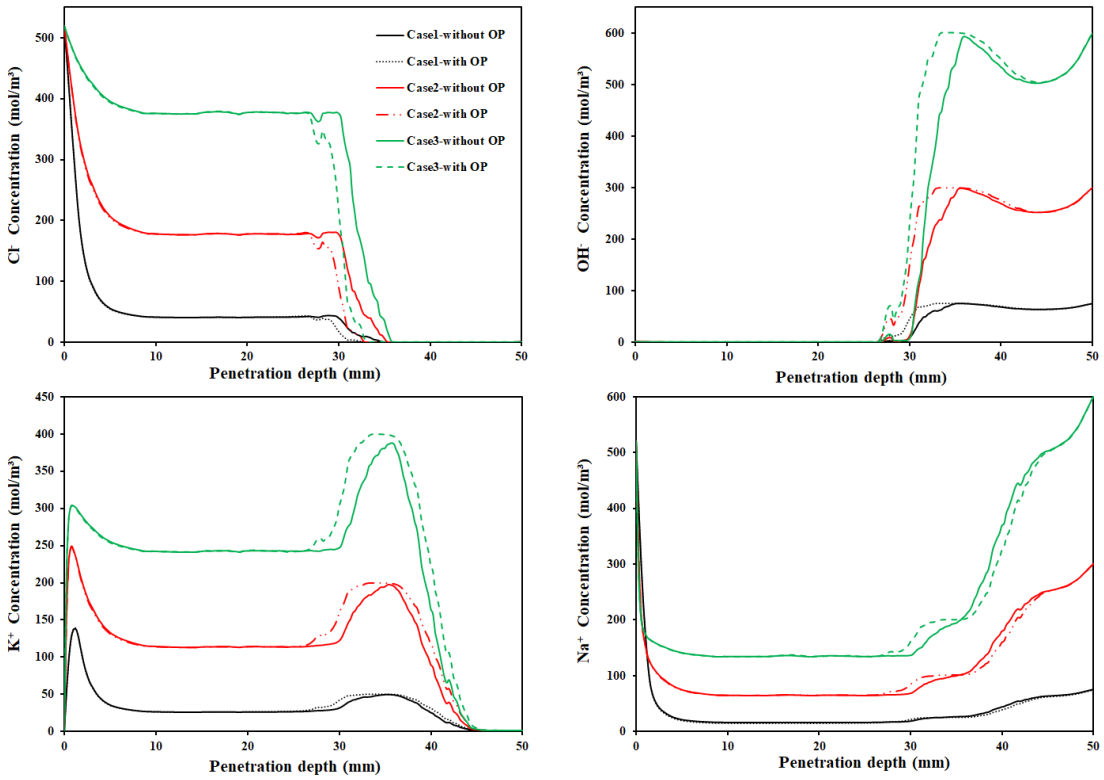

Figure 14 Concentration distribution profiles of Cl^-, OH^-, K^+, Na^+ ions in the cases with and without considering the overpotential (OP) when three different initial concentrations applied.

6. Conclusions

A numerical simulation model, considering multi-species transport, polarization at electrodes and non-equilibrium chloride binding, has been developed to describe the variation of electric potential at concrete surfaces and its effects on ionic transportation in concrete during the electrochemical processes. Based on the results obtained from the present study, the following conclusions can be drawn.

1. With consideration of the overpotentials at electrodes, the potential drop across the concrete specimen is 7~25% lower than that applied between the two electrodes in different cases, leading to the decreased chloride penetration depth.
2. The total overpotential at electrode-electrolyte interfaces gradually decreases due to the decrease of current density flow through concrete during the RCM test. However, the effect of overpotential on the concentration distribution of individual ionic species seems obvious and increases with time.

3. The total overpotential appears to be lightly dependent on the externally applied voltage and the initial concentration of ions in concrete. However, the Tafel parameters describing the electrochemical reactions on the cathode and anode have a great influence on the change of overpotential.
4. The effect of overpotential on ionic transport is determined by both the magnitude of it and the proportion of it to the externally applied voltage. The higher the externally applied voltage, the more minor effect of overpotential on the chloride penetration.
5. The larger the Tafel slope, the higher the overpotential, and the stronger the effect on the ionic transport. Conversely, the high exchange current density used in the present overpotential model will decrease the value of overpotential and slightly increase the penetration depth of chloride ions.
6. The initial concentration of ions in pore solution has a limited effect on the overpotential and ingress depth of chloride ions. Nevertheless, the total amount of penetrated chloride ions shows a noticeable increment with the increase of the initial concentration.

References

[1] G. Narsilio, R. Li, P. Pivonka, D. Smith, Comparative study of methods used to estimate ionic diffusion coefficients using migration tests, Cement and Concrete Research 37(8) (2007) 1152-1163.
[2] H.M. Oleiwi, Y. Wang, M. Curioni, X. Chen, G. Yao, L. Augusthus-Nelson, A. Ragazzon-Smith, I. Shabalin, An experimental study of cathodic protection for chloride contaminated reinforced concrete, Materials and structures 51 (2018) 148.
[3] J.M. Paz-García, B. Johannesson, L.M. Ottosen, A.N. Alshawabkeh, A.B. Ribeiro, J.M. Rodríguez-Maroto, Modeling of electrokinetic desalination of bricks, Electrochimica acta 86 (2012) 213-222.
[4] Y. Tissier, V. Bouteiller, E. Marie-Victoire, S. Joiret, T. Chaussadent, Y. Tong, Electrochemical chloride extraction to repair combined carbonated and chloride contaminated reinforced concrete, Electrochimica Acta 317 (2019) 486-493.
[5] Y.-S. Chen, M.-C. Li, Y.-W. Chan, C.-C. Yang, The relationship between accelerated migration time in ACMT and ponding time in ponding test for cement-based materials, Journal of Marine Science and Technology 20(1) (2012) 1-8.
[6] T. Luping, L.-O. Nilsson, Rapid determination of the chloride diffusivity in concrete by applying an electric field, Materials Journal 89(1) (1993) 49-53.

[7] NT BUILD 492, Concrete, mortar and cement-based repair materials: chloride migration coefficient from non-steady-state migration experiments, Published by NORDTEST, P.O. Box 116, FIN－02151 ESPOO, FINLAND, 1999.
[8] P. McGrath, R. Hooton, Influence of voltage on chloride diffusion coefficients from chloride migration tests, Cement and concrete research 26(8) (1996) 1239-1244.
[9] D. Aikens, Electrochemical methods, fundamentals and applications, American Chemical Society, Washington, D.C, 1983.
[10] P. Spiesz, H. Brouwers, Influence of the applied voltage on the Rapid Chloride Migration (RCM) test, Cement and Concrete Research 42(8) (2012) 1072-1082.
[11] J. Xia, L.-y. Li, Numerical simulation of ionic transport in cement paste under the action of externally applied electric field, Construction and Building Materials 39 (2013) 51-59.
[12] B. Guo, G. Qiao, D. Li, J. Ou, Multi-species reactive transport modeling of electrochemical corrosion control in saturated concrete structures including electrode reactions and thermodynamic equilibrium, Construction and Building Materials 278 (2021) 122228.
[13] G. Glass, The 100-mV potential decay cathodic protection criterion, Corrosion 55(3) (1999) 286-290.
[14] G. Qiao, B. Guo, J. Ou, F. Xu, Z. Li, Numerical optimization of an impressed current cathodic protection system for reinforced concrete structures, Construction and Building Materials 119 (2016) 260-267.
[15] E. Muehlenkamp, M. Koretsky, J. Westall, Effect of moisture on the spatial uniformity of cathodic protection of steel in reinforced concrete, Corrosion 61(6) (2005) 519-533.
[16] C. Protection, Part 1, Code of Practice for Land and Marine Applications, British Standard, Englewood, Colorado, 1991.
[17] A. Hassanein, G. Glass, N. Buenfeld, Protection current distribution in reinforced concrete cathodic protection systems, Cement and Concrete Composites 24(1) (2002) 159-167.
[18] C. Helm, M. Raupach, Development of a numerical simulation model considering the voltage drops within CP anode systems in RC structures: Dedicated to Dr. Jürgen Mietz on the occasion of his 60th birthday, Materials and Corrosion 67 (2016) 621-630.
[19] J.L. Marriaga, P. Claisse, Effect of the non-linear membrane potential on the migration of ionic species in concrete, Electrochimica Acta 54(10) (2009) 2761-2769.
[20] G. Skibsted, L.M. Ottosen, P.E. Jensen, J.M. Paz-Garcia, Electrochemical desalination of bricks－Experimental and modeling, Electrochimica Acta 181 (2015) 24-30.
[21] E. Samson, J. Marchand, J. Beaudoin, Describing ion diffusion mechanisms in cement-based materials using the homogenization technique, Cement and Concrete Research 29(8) (1999) 1341-1345.
[22] E. Samson, J. Marchand, K.A. Snyder, Calculation of ionic diffusion coefficients on the basis of migration test results, Materials and structures 36(3) (2003) 156-165.

[23] O. Truc, J.-P. Ollivier, L.-O. Nilsson, Numerical simulation of multi-species transport through saturated concrete during a migration test—MsDiff code, Cement and Concrete Research 30(10) (2000) 1581-1592.
[24] K. Krabbenhøft, J. Krabbenhøft, Application of the Poisson-Nernst-Planck equations to the migration test, Cement and Concrete Research 38(1) (2008) 77-88.
[25] B. Johannesson, Development of a generalized version of the Poisson-Nernst-Planck equations using the hybrid mixture theory: presentation of 2D numerical examples, Transport in Porous Media 85(2) (2010) 565-592.
[26] B. Johannesson, Comparison between the Gauss' law method and the zero current method to calculate multi-species ionic diffusion in saturated uncharged porous materials, Computers and Geotechnics 37(5) (2010) 667-677.
[27] J.M. Paz-Garcia, B. Johannesson, L.M. Ottosen, A. Ribeiro, J. Rodríguez-Maroto, Simulation-based analysis of the differences in the removal rate of chlorides, nitrates and sulfates by electrokinetic desalination treatments, Electrochimica Acta 89 (2013) 436-444.
[28] Q.-f. Liu, J. Yang, J. Xia, D. Easterbrook, L.-y. Li, X.-Y. Lu, A numerical study on chloride migration in cracked concrete using multi-component ionic transport models, Computational Materials Science 99 (2015) 396-416.
[29] Q.-f. Liu, G.-l. Feng, J. Xia, J. Yang, L.-y. Li, Ionic transport features in concrete composites containing various shaped aggregates: a numerical study, Composite Structures 183 (2018) 371-380.
[30] L.-x. Mao, Z. Hu, J. Xia, G.-l. Feng, I. Azim, J. Yang, Q.-f. Liu, Multi-phase modelling of electrochemical rehabilitation for ASR and chloride affected concrete composites, Composite Structures 207 (2019) 176-189.
[31] S.D. Abyaneh, H. Wong, N. Buenfeld, Modelling the diffusivity of mortar and concrete using a three-dimensional mesostructure with several aggregate shapes, Computational Materials Science 78 (2013) 63-73.
[32] L.-y. Li, D. Easterbrook, J. Xia, W.-L. Jin, Numerical simulation of chloride penetration in concrete in rapid chloride migration tests, Cement and Concrete Composites 63 (2015) 113-121.
[33] P. Yang, G. Sant, N. Neithalath, A refined, self-consistent Poisson-Nernst-Planck (PNP) model for electrically induced transport of multiple ionic species through concrete, Cement and Concrete Composites 82 (2017) 80-94.
[34] Y. Liu, X. Shi, Ionic transport in cementitious materials under an externally applied electric field: Finite element modeling, Construction & Building Materials 27 (2012) 450-460.
[35] L. Hourng, T. Tsai, M. Lin, The analysis of energy efficiency in water electrolysis under high temperature and high pressure, IOP Conference Series: Earth and Environmental Science, IOP Publishing, 2017, pp. 012035.
[36] M. Pour-Ghaz, O.B. Isgor, P. Ghods, The effect of temperature on the corrosion of steel in concrete. Part 1: Simulated polarization resistance tests and model development, Corrosion Science 51(2) (2009) 415-425.
[37] T. Shinagawa, A.T. Garcia-Esparza, K. Takanabe, Insight on Tafel slopes from a microkinetic analysis of aqueous electrocatalysis for energy conversion, Scientific

reports 5 (2015) 13801.
[38] M. Brem, Numerische Modellierung der Korrosion in Stahlbetonbauten: Anwendung der Boundary Element Methode, ETH Zurich, 2004.
[39] J. Warkus, M. Raupach, Numerical modelling of macrocells occurring during corrosion of steel in concrete, Materials and corrosion 59(2) (2008) 122-130.
[40] J. Xia, T. Li, J.-X. Fang, W.-l. Jin, Numerical simulation of steel corrosion in chloride contaminated concrete, Construction and Building Materials 228 (2019) 116745.
[41] Y. Wang, C. Liu, Y. Wang, Q. Li, B. Yan, Semi-empirical prediction model of chloride-induced corrosion rate in uncracked reinforced concrete exposed to a marine environment, Electrochimica Acta 331 (2020) 135376.
[42] Y.-H. Fang, Z.-P. Liu, Tafel kinetics of electrocatalytic reactions: from experiment to first-principles, ACS Catalysis 4 (2014) 4364-4376.
[43] J.K. Nørskov, T. Bligaard, A. Logadottir, J. Kitchin, J.G. Chen, S. Pandelov, U. Stimming, Trends in the exchange current for hydrogen evolution, Journal of The Electrochemical Society 152(3) (2005) J23.
[44] J. Nai, Y. Lu, L. Yu, X. Wang, X.W. Lou, Formation of Ni-Fe mixed diselenide nanocages as a superior oxygen evolution electrocatalyst, Advanced Materials 29 (2017) 1703870.
[45] U.G. Akano, Oxygen Evolution Reactions on Nickel, Nickel Oxide Electrodes Using Galvanostatic Methods, Master Thesis, McMaster University, 1980.
[46] D.W. Green, M.Z. Southard, Perry's Chemical Engineers' handbook, McGraw-Hill Education, New York, 2019.
[47] P. Spiesz, M. Ballari, H. Brouwers, RCM: a new model accounting for the non-linear chloride binding isotherm and the non-equilibrium conditions between the free- and bound-chloride concentrations, Construction and Building Materials 27(1) (2012) 293-304.
[48] E. Theissing, P. Hest-Wardenier, G. De Wind, The combining of sodium chloride and calcium chloride by a number of different hardened cement pastes, Cement and Concrete Research 8(6) (1978) 683-691.
[49] L. Tang, Chloride transport in concrete-measurement and prediction, Chalmers University of Technology, Sweden, PhD Thesis, 1996.
[50] V. Baroghel-Bouny, P. Belin, M. Maultzsch, D. Henry, AgNO 3 spray tests: advantages, weaknesses, and various applications to quantify chloride ingress into concrete. Part 2: Non-steady-state migration tests and chloride diffusion coefficients, Materials and structures 40(759) (2007) 783-799.
[51] V. Baroghel-Bouny, K. Kinomura, M. Thiery, S. Moscardelli, Easy assessment of durability indicators for service life prediction or quality control of concretes with high volumes of supplementary cementitious materials, Cement and Concrete Composites 33(8) (2011) 832-847.
[52] Y. Cao, L. Guo, B. Chen, J. Wu, Thermodynamic modelling and experimental investigation on chloride binding in cement exposed to chloride and chloride-sulfate solution, Construction and Building Materials 246 (2020) 118398.
[53] Q.-f. Liu, D. Easterbrook, J. Yang, L.-y. Li, A three-phase, multi-component

ionic transport model for simulation of chloride penetration in concrete, Engineering Structures 86 (2015) 122-133.
[54] B. Šavija, M. Luković, E. Schlangen, Lattice modeling of rapid chloride migration in concrete, Cement and Concrete Research 61 (2014) 49-63.
[55] L.Y. Li, P. Bettess, J. Bull, T. Bond, I. Applegarth, Theoretical formulations for adaptive finite element computations. Communications in Numerical Methods in Engineering 11(10) (1995) 857-868.
[56] J. Haverkort, H. Rajaei, Electro-osmotic flow and the limiting current in alkaline water electrolysis, Journal of Power Sources Advances 6 (2020) 100034.
[57] L. Jiang, Z. Song, H. Yang, Q. Pu, Q. Zhu, Modeling the chloride concentration profile in migration test based on general Poisson Nernst Planck equations and pore structure hypothesis, Construction and Building Materials 40 (2013) 596-603.
[58] M. Castellote, C. Andrade, C. Alonso, Chloride-binding isotherms in concrete submitted to non-steady-state migration experiments, Cement and Concrete Research 29(11) (1999) 1799-1806.
[59] Q. Yuan, D. Deng, C. Shi, G. De Schutter, Chloride binding isotherm from migration and diffusion tests, Journal of Wuhan University of Technology (Mater. Sci. ed.) 28 (2013) 548-556.